

Ultrahigh-Q circular-side square resonator lasers with enhanced transverse mode interval

Hai-Zhong Weng, Yong-Zhen Huang,* Yue-De Yang, Xiu-Wen Ma, Jin-Long Xiao, and Yun Du

State Key laboratory on Integrated Optoelectronics, Institute of Semiconductors,

Chinese Academy of Sciences, Beijing, 100083, China

A mechanism of transverse mode control is proposed for circular-side square resonator (CSR) with the flat sides replaced by arcs, which results in ultrahigh- Q factors and large transverse mode intervals according to two and three dimensional (2D and 3D) simulations. A 2D numerical optimization shows that mode Q factors up to 10^{11} can be obtained for the 16- μm -side-length CSR with a 1.5- μm -width output waveguide. Dual-mode lasing with frequency intervals in THz range in agreement with simulated results is achieved for AlGaInAs/InP CSR lasers.

Optical microresonators that exploit total internal reflection (TIR) of light ray can have high quality (Q) whispering-gallery modes (WGMs). High- Q microcavities with strong concentrate capability of light are full of importance for fundamental physics studies and practical optoelectronic devices [1]. Microdisks and microrings as the most common WGM resonators have been extensively investigated for the applications in nonlinear optics [2, 3], light-matter coupling study [4, 5], optical add-drop filters [6, 7], and microlasers [8, 9], etc. With the advantages of small mode volume and low power consumption, WGM microlasers are attracted as potential light sources for on-chip optical interconnection and photonic integrated circuits [10-12]. Deformed circular [13-15] and sphere [16] resonators with high- Q modes have been studied to realize low threshold directional emission microlasers, and mode Q factors up to 10^8 are expected for an unidirectional emission deformed circular resonator based on dynamical tunneling [17]. In addition to microdisks, square resonators have also been investigated to fabricate directional emission microlasers [18-24]. Widely tunable single-mode lasing is realized using the middle-point output waveguide for mode selection [24]. However, the mode Q factors of the square microresonator are greatly limited by the inevitable radiation loss from the vertices of the square resonator.

In this letter, we report a novel circular-side square resonator (CSR), with the flat-sides replaced by arcs as concave reflectors for the WGMs. The transverse waveguiding effect of the concave reflectors can converge the mode light rays along a narrow transmission path, which results in ultrahigh- Q WGMs due to the elimination of the vertices radiation loss. Furthermore, the converged effects can greatly enhance the transverse mode intervals with suitable arc-radius. Therefore, it is interesting to explore the possibility to combine the high- Q factor and large mode spacing, which are particularly crucial for new dual-mode or multi-mode lasing devices. In addition, the CSRs are easy to realize in practice without complicated design or sophisticated fabrication process. The uniform dual-transverse-mode lasing is experimentally demonstrated for CSR microlasers, with wavelength intervals in agreement with numerical simulations, which can be utilized for terahertz (THz) wave generation by optical heterodyne technique.

The 2D CSR as shown in the inset of Fig. 1(a) is considered with the flat sides (dashed lines) replaced by circular arcs and connected to an output waveguide at one vertex. The side-length of the resonator and the width of the output waveguide are a and w , respectively, while the arc-radius r is greater than $a/\sqrt{2}$. Deformation amplitude δ defined as $r - \sqrt{r^2 - a^2/4}$ is depicted in the inset. Solving the wave equation by finite element method (FEM, COMSOL Multiphysics 5.0), we investigate the influence of the deformation on the mode characteristics, for the CSRs surrounded by bisbenzo cyclobutene (BCB). Taking $a = 16 \mu\text{m}$, $w = 1.5 \mu\text{m}$, and the refractive indices of 3.2 and 1.54 for the CSR and the BCB, respectively, we simulate the transverse electric (TE) modes with z -direction magnetic field H_z satisfying symmetric condition relative to the centreline of the output waveguide.

Resonance wavelengths and Q factors of the symmetric TE modes versus the deformation amplitude δ are calculated and plotted in Figs. 1(a) and 1(b), respectively. The mode wavelength of the fundamental mode increases linearly with the increase of δ , while the wavelengths of the first-order and second-order modes increase oscillatorily. Contrary to the flat-side square microcavity [23], the high order transverse modes have larger mode wavelengths than the fundamental mode as $1.05 \leq \delta \leq 1.5 \mu\text{m}$. The wavelength difference $\Delta\lambda$ between the fundamental transverse mode and the first-order transverse mode reaches the magnitude of 4.04, 2.69, and 1.48 nm as $\delta = 1.1$, 1.3, and 1.5 μm , respectively, much larger than the one of 1.05 nm as $\delta = 0$. The Q factors of the fundamental, first-order, and second-order transverse modes are 1.2×10^4 , 2.3×10^3 , and 2×10^3 , respectively, as $\delta = 0$, then rapidly increase to 2.5×10^9 , 7.5×10^7 , and 7×10^6 , as δ increases to 0.5 μm , and drop to 5.2×10^3 , 3.6×10^3 , and 3×10^3 as $\delta = 0.9 \mu\text{m}$, and finally increase to the maximum values of 1.3×10^{11} , 2.1×10^{10} , and 1.4×10^9 as $\delta = 1.3 \mu\text{m}$.

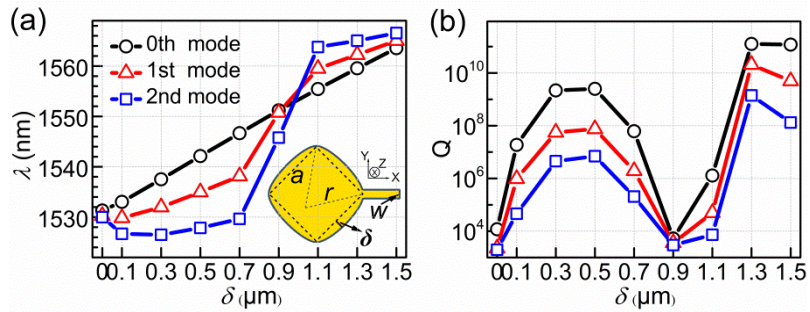


FIG. 1 (a) Resonance wavelengths and (b) mode Q factors versus the deformation amplitude δ . The fundamental, first-order and second-order symmetric transverse modes are marked by \circ , Δ , and \square , respectively. Inset: Schematic structure of the circular-side square resonator with an output waveguide at one vertex.

Mode field distributions of the magnetic field component $|H_z|$ are presented in Figs. 2(a)-2(d) for the fundamental modes and in Figs. 2(e)-2(h) for the first-order modes as $\delta = 0, 0.5, 0.9$, and $1.3 \mu\text{m}$, respectively. Distributions on the right side including the output waveguide are magnified by two times. The mode field patterns are nearly uniformly distributed in Figs. 2(a) and 2(e) for the flat-side square resonator, which have strong coupling efficiency to the output waveguide and large radiation loss in the vertices of the square. At $\delta = 0.5 \mu\text{m}$, the mode fields are well confined in the transverse direction with obvious quadrilateral patterns as shown in Figs. 2(b) and 2(f), resulting in the reduction of radiation loss at

the vertices. At $\delta = 0.9 \mu\text{m}$, the mode fields in Figs. 2(c) and 2(g) distribute over the whole resonator and have a very large radiation loss, corresponding to the minimum mode Q factors in Fig. 1(b). As is shown in Figs. 2(d) and 2(h), mode fields are compressed better again at $\delta = 1.3 \mu\text{m}$ with a more narrow transmission path. Therefore, we can conclude that the ultrahigh- Q factors and large transverse mode intervals can be obtained simultaneously for the CSR at suitable arc-radius due to the convergence of optical beam.

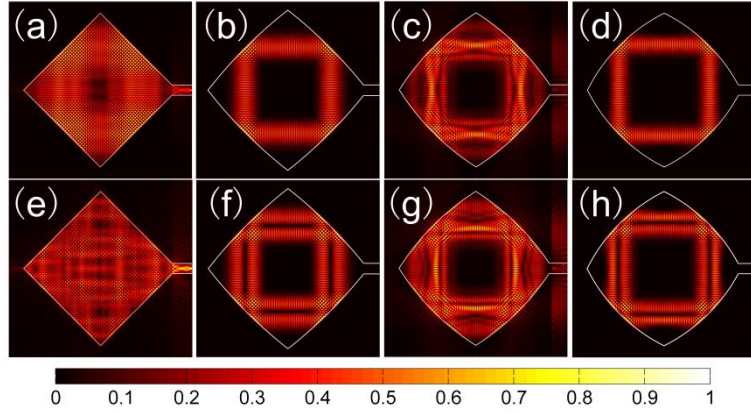


FIG. 2 Distributions of magnetic field component $|H_z|$ for the fundamental (a)-(d) and first-order transverse modes (e)-(h) with the deformation amplitude δ of 0, 0.5, 0.9, and $1.3 \mu\text{m}$, respectively. The fields on the right side including the output waveguide are magnified by two times for clear illustration.

In order to confirm the numerical simulations, CSR lasers with $a = 16 \mu\text{m}$, $w = 1.5 \mu\text{m}$ are fabricated with $\delta = 1.1$, 1.3 , and $1.5 \mu\text{m}$, respectively. The microlasers are fabricated on an AlGaInAs/InP wafer with eight pairs of compressively strained multiple-quantum-wells, using the technical process as in [24, 25]. The insets in Figs. 3(a) and 3(b) show the side-view scanning electron microscope (SEM) image after inductively coupled-plasma (ICP) etching and top-view microscope image of a fabricated microlaser, respectively. The CSR lasers are tested at the temperature of 288 K by butt-coupling a multi-mode fiber to the cleaving facet of the output waveguide. Collected powers versus continuous-wave (CW) injection current (L - I) are plotted in Fig. 3(a) as the solid, dashed and dashed-dotted lines at $\delta = 1.1$, 1.3 , and $1.5 \mu\text{m}$, respectively. The threshold currents are 6, 7, and 7 mA, respectively, and maximum powers are 52, 28, and $34 \mu\text{W}$ at 34, 39, and 43 mA, respectively.

Lasing spectra at 31 mA are plotted in Figs. 3(b)-3(d) for the lasers at $\delta = 1.1$, 1.3 , and $1.5 \mu\text{m}$, respectively. With the help of the numerical calculation, the fundamental, first-order, second-order, and third-order transverse modes are assigned and marked by the circle, triangle, square, and pentagram symbols, respectively. Two main transverse modes lasing simultaneously are clearly observed with the wavelengths of 1553.84, 1552.44, 1555.25 nm for the fundamental transverse mode, and 1557.27, 1554.9, 1556.51 nm for the first-order mode, as $\delta = 1.1$, 1.3 , and $1.5 \mu\text{m}$, respectively. Corresponding mode intervals of 3.43, 2.46, and 1.26 nm are in good agreement with the calculated values 4.04, 2.69, and 1.48 nm. The intensity ratios between the two lasing modes are 0.5, 0.2, and 0.5 dB, and the other modes are 27,

23, and 25 dB less than the lasing modes, respectively. Evident multi-resonance peaks verify the high- Q factors for the CSR, which can also reduce the lasing threshold. Lasing spectra from 25 to 38 mA are plotted in Fig. 3(e), showing uniform dual-transverse-mode operations. The red-shifts of the lasing wavelengths are attributed to an injection current-induced thermal effect, and the wavelength shifts of the fundamental modes near 1553 nm are proportional to the injection current at the slopes of 0.108, 0.113, and 0.112 nm/mA, as $\delta = 1.1$, 1.3, and 1.5 μm , respectively. According to the variation of the mode wavelength with the temperature 0.115 nm/K [25], the thermal heating effects are estimated at the slopes of 0.94, 0.98, and 0.97 K/mA, respectively. The injection current-induced thermal effect also results in the shift of the gain spectra, and thus leads to the mode-hopping with a longitudinal mode interval of 13 nm as the injection is larger than 35 mA. The fundamental and first-order transverse modes are marked by the solid and dashed arrows, respectively, and the corresponding intensity ratios are less than 2 dB from 27 to 35 mA. The mode wavelength intervals are maintained at 3.43, 2.46, and 1.26 nm as $\delta = 1.1$, 1.3, and 1.5 μm , respectively.

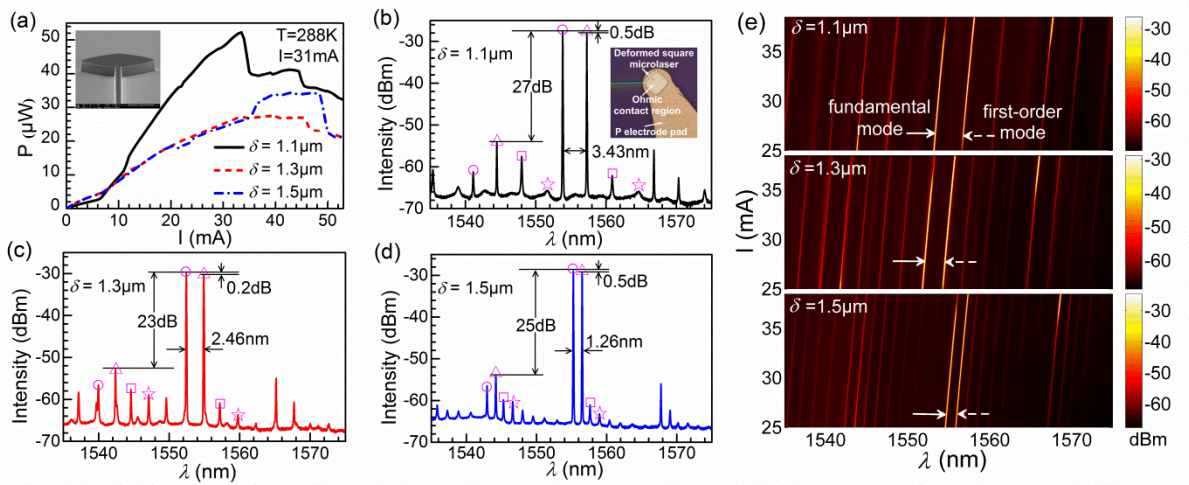


FIG. 3 (a) Fiber coupled output powers versus CW injection current for the lasers with δ of 1.1, 1.3, and 1.5 μm . Inset: a side-view SEM image after ICP technique. (b) - (d) Lasing spectra at the injection current of 31 mA for the CSR lasers with δ of 1.1, 1.3, and 1.5 μm , respectively, showing dual-transverse-mode operations around 1555 nm. The fundamental, first-order, second-order, and third-order transverse modes are marked by \circ , Δ , \square , and \star , respectively. Inset: top-view microscope image of a fabricated microlaser. (e) Wavelength map of the lasing spectra from 25 to 38 mA at 288 K for the lasers. The fundamental and first-order modes are indicated with the solid and dashed arrows, respectively.

The THz radiation sources with ultra-compact structure and simplified fabrication technique are greatly demanded for the chip interconnection and the wireless network [26, 27]. Thus we demonstrate the potential generation of THz beating signals from the CSR lasers by using the noncollinear intensity autocorreclator [28, 29]. As is shown in Fig. 4(a), the dual-mode output signal of the CSR microlaser is pre-amplified by an erbium-doped fiber amplifier (EDFA). Then the amplified output is filtered by a tunable optical band-pass filter (OBPF), and split up two parts with 1% of the light for monitoring the optical spectra and 99% of the light are amplified and injected to the auto-correlator to detect the beating frequency after the fiber polarization controller (FPC). Autocorrelation pulse trains are plotted in Fig. 4(b)

for the CSR lasers operated at 31 mA. The sinusoidal modulation signals of the pulse trains have the average periods of 2.34, 3.22, and 6.44 ps as $\delta = 1.1$, 1.3, and 1.5 μm , respectively, corresponding to the beating frequencies of 0.43, 0.31, and 0.16 THz.

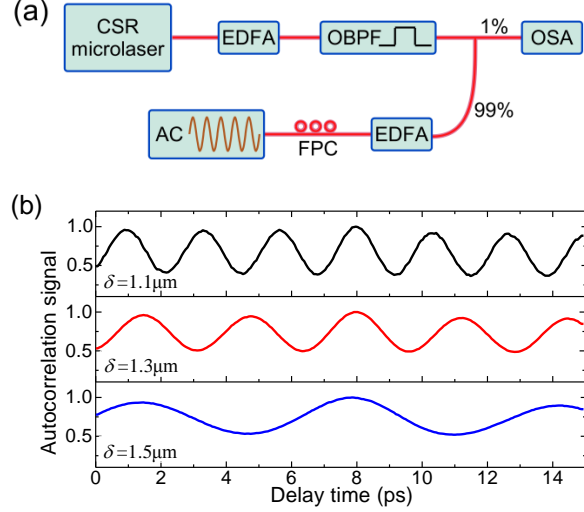


FIG. 4 Autocorrelation measurements based on the dual-mode CSR microlasers. (a) Experimental setup. (b) Measured autocorrelation pulse trains for the lasers with δ of 1.1, 1.3 and 1.5 μm , respectively, at 31mA and 288K. EDFA, erbium-doped fiber amplifier; OBPF, optical band-pass filter; OSA, optical spectral analyzer, FPC, fiber polarization controller; AC, auto-correlator.

Finally, we verify the enhanced mode Q factors for 3D silicon CSR without an output waveguide, consisted of a 220 nm thick silicon layer sandwiched between two 1.5 μm thick SiO_2 confinement layers. The microresonator with $a = 6 \mu\text{m}$ is analysed with the refractive indices for silicon and SiO_2 of 3.48 and 1.45, respectively. The symmetry of the magnetic field H_z in the x - y plane can be classified as four types $[x, y] = [\pm, \pm]$, with “+” and “-” represent symmetric and antisymmetric relative to the square diagonal mirror planes $x = 0$ or $y = 0$. Considering the TE modes with H_z symmetric to the plane of $z = 0$, we simulate the mode characteristics by the FEM in the eighth of the 3D resonator based on the symmetry conditions. The mode wavelengths and Q factors of the fundamental transverse modes versus δ are plotted in Fig. 5 as the open and solid symbols, respectively, for the modes with the symmetry of $[+, +]$, $[+, -]$, and $[-, -]$. The resonance wavelengths are red-shift with the increase of δ as the 2D case in Fig. 1(a). The anti-symmetric mode with the symbol $[-, -]$ has the Q -factor one order larger than the other modes at $\delta = 0$, because of the less scattering loss in the vertices [24]. The Q factors increase about two orders to 2×10^5 , of the same magnitude as the $[-, -]$ mode, for the $[+, +]$ and $[+, -]$ modes as δ increases from zero to 0.1 μm . In addition, the mode field patterns are also analogous to the 2D simulations, which further confirm the transverse waveguiding effect.

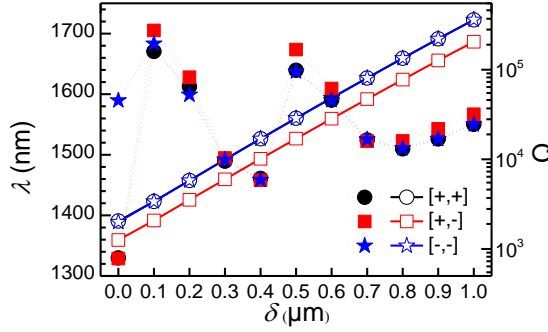


FIG. 5 Resonance wavelengths (open symbols) and Q factors (solid symbols) versus δ , for the TE fundamental mode with symmetry of $[+, +]$, $[+, -]$, and $[-, -]$ in the x - y plane.

In summary, we have demonstrated a novel circular-side square resonator with ultrahigh- Q factors and enhanced transverse mode intervals. The circular-sides can confine the mode pattern and eliminate the vertex radiation loss. Mode Q factors up to 10^{11} are expected for the resonator connected an output waveguide with the side-length of $16 \mu\text{m}$. The ultrahigh- Q factors for the CSR with an output waveguide provide a multifunction component for potential complicated photonic integrated circuits. Stable dual-transverse-mode lasing with the wavelength intervals in good agreement with the simulation results are achieved for AlGaInAs/InP CSR lasers. Furthermore, the beating signals of 0.43, 0.31, and 0.16 THz are obtained by the autocorrelation traces, which indicate the CSR lasers as a novel architecture for THz radiation generation.

We acknowledge the support from the National Natural Science Foundation of China under Grant Nos. 61527823, 61235004, 61321063, and 61376048.

*yzhuang@semi.ac.cn

- [1] K.J. Vahala, *Nature* **424**, 839 (2003).
- [2] T.J. Kippenberg, S.M. Spillane, and K.J. Vahala, *Phys. Rev. Lett.* **93**, 083904 (2004).
- [3] T.J. Johnson, M. Borselli, and O. Painter, *Opt. Express* **14**, 817 (2006).
- [4] C. Junge, D. O'Shea, J. Volz, and A. Rauschenbeutel, *Phys. Rev. Lett.* **110**, 213604 (2013).
- [5] S.M. Grist, S.A. Schmidt, J. Flueckiger, V. Donzella, W. Shi, S. Talebi Fard, J.T. Kirk, D.M. Ratner, K.C. Cheung, and L. Chrostowski, *Opt. Express* **21**, 7994 (2013).
- [6] S. Xiao, M.H. Khan, H. Shen, and M. Qi, *J. Lightwave Technol.* **26**, 228 (2008).
- [7] A.W. Poon, X.S. Luo, F. Xu, and H. Chen, *Pro. IEEE* **97**, 1216 (2009).
- [8] S.L. McCall, A.F.J. Levi, R.E. Slusher, S.J. Pearton, and R.A. Logan, *Appl. Phys. Lett.* **60**, 289 (1992).
- [9] X.M. Lv, Y.Z. Huang, L.X. Zou, H. Long, and Y. Du, *Laser Photon. Rev.* **7**, 818 (2013).
- [10] L. He, S.K. Özdemir, and L. Yang, *Laser Photon. Rev.* **7**, 60 (2013).
- [11] H.T. Hattori, C. Seassal, E. Touraille, P. Rojo-Romeo, X. Letartre, G. Hollinger, P. Viktorovitch, L. Di Cioccio, M. Zussy, L.E. Melhaoui, and J.M. Fedeli, *IEEE Photon. Tech. Lett.* **18**, 223 (2006).
- [12] J. Wiersig and M. Hentschel, *Phys. Rev. Lett.* **100**, 033901 (2008).

[13] J. Yang, S. B. Lee, S. Moon, S. Y. Lee, S. W. Kim, T. T. A. Dao, J.H. Lee, and K An, *Phys. Rev. Lett.* **104**, 243601 (2010).

[14] C.L Zou, F.W. Sun, C.H. Dong, F.J. Shu, X.W. Wu, J.M. Cui, Y. Yang, Z.F Han, and G.C. Guo, *IEEE J. Sel. Topics Quantum Electron.* **19**, 9000406 (2013).

[15] X.F. Jiang, Y.F. Xiao, C.L. Zou, L. He, C.H. Dong, B.B. Li, Y. Li, F.W. Sun, L. Yang, and Q. Gong, *Adv. Mater.* **24**, OP260 (2012).

[16] S. Lacey, H. Wang, D.H. Foster, and J.U. Nöckel, *Phys. Rev. Lett.* **91**, 033902 (2003).

[17] Q.H. Song, L. Ge, B. Redding, and H. Cao, *Phys. Rev. Lett.* **108**, 243902 (2012).

[18] H.J. Moon, K. An, and J.H. Lee, *Appl. Phys. Lett.* **82**, 2963 (2003).

[19] S.V. Boriskina, T.M. Benson, P. Sewell, and A.I. Nosich, *J. Opt. Soc. Am. B* **21**, 1792 (2004).

[20] W.H. Guo, Y.Z. Huang, Q.Y. Lu, and L.J. Yu, *IEEE J. Quantum Electron.* **39**, 1563 (2003).

[21] C.W. Lee, Q. Wang, Y. Lai, D.K.T. Ng, and S.K. Ng, *IEEE Photon. Tech. Lett.* **26**, 2442 (2014).

[22] Y.Z. Huang, K.J. Che, Y.D. Yang, S.J. Wang, Y. Du, and Z.C. Fan, *Opt. Lett.* **33**, 2170 (2008).

[23] M.Y. Tang, S.S. Sui, Y.D. Yang, J.L. Xiao, Y. Du, and Y.Z. Huang, *Opt. Express* **23**, 27739 (2015).

[24] H. Long, Y.Z. Huang, X.W. Ma, Y.D. Yang, J.L. Xiao, L.X. Zou, and B.W. Liu, *Opt. Lett.* **40**, 3548 (2015).

[25] L.X. Zou, Y.Z. Huang, B.W. Liu, X.M. Lv, X.W. Ma, Y.D. Yang, J.L. Xiao, and Y. Du, *Opt. Express* **23**, 2879 (2015).

[26] S. Koenig, D. Lopez Diaz, J. Antes, F. Boes, R. Henneberger, A. Leuther, A. Tessmann, R. Schmogrow, D. Hillerkuss, R. Palmer, T. Zwick, C. Koos, W. Freude, O. Ambacher, J. Leuthold, and I. Kallfass, *Nat Photon.* **7**, 977 (2013).

[27] H.J. Song and T. Nagatsuma, *IEEE Trans. Terahertz Sci. Technol.* **1**, 256 (2011).

[28] M. Uemukai, H. Ishida, A. Ito, T. Suhara, H. Kitajima, A. Watanabe, and H. Kan, *Jpn. J. Appl. Phys.* **51**, 020205 (2012).

[29] N. Kim, J. Shin, E. Sim, C.W. Lee, D.S. Yee, M.Y. Jeon, Y. Jang, and K.H. Park, *Opt. Express* **17**, 13851 (2009).